Mon. Not. R. Astron. Soc. **000**, 1–5 (2015) Printed 12 April 2016 (MN LATEX style file v2.2)

First Detection of $^3He^+$ in the Planetary Nebula IC 418

L. Guzman-Ramirez[1,2⋆], J. R. Rizzo[3], A. A. Zijlstra[4], C. García-Miró[5], C. Morisset[6] & M. D. Gray[4]

[1]*European Southern Observatory, Alonso de Córdova 3107, Casilla 19001, Santiago, Chile*
[2]*Leiden Observatory, Leiden University, Niels Bohrweg 2, 2333 CA Leiden, The Netherlands*
[3]*Centro de Astrobiología (INTA-CSIC), Ctra. M-108, km. 4, 28850, Torrejón de Ardoz, Spain*
[4]*Jodrell Bank Centre for Astrophysics, School of Physics and Astronomy, University of Manchester, Manchester, M13 9PL, UK*
[5]*Madrid Deep Space Communications Complex, Ctra. M-531, km. 7, E-28294 Robledo de Chavela, Madrid, Spain*
[6]*Instituto de Astronomía, Universidad Nacional Autónoma de México, 04510 México D.F., México*

Accepted 2016 xxx. Received 2015 xxx; in original form 2015 xxx

ABSTRACT

The ^{3}He isotope is important to many fields of astrophysics, including stellar evolution, chemical evolution, and cosmology. The isotope is produced in low-mass stars which evolve through the planetary nebula (PN) phase. ^{3}He abundances in PNe can help test models of the chemical evolution of the Galaxy. We present the detection of the $^3He^+$ emission line using the single dish Deep Space Station 63, towards the PN IC 418. We derived a ^{3}He/H abundance in the range $1.74\pm0.8\times10^{-3}$ to $5.8\pm1.7\times10^{-3}$, depending on whether part of the line arises in an outer ionized halo. The lower value for ^{3}He/H ratio approaches values predicted by stellar models which include thermohaline mixing, but requires that large amounts of ^{3}He are produced inside low-mass stars which enrich the interstellar medium (ISM). However, this over-predicts the ^{3}He abundance in H II regions, the ISM, and proto-solar grains, which is known to be of the order of 10^{-5}. This discrepancy questions our understanding of the evolution of the ^{3}He, from circumstellar environments to the ISM.

Key words: circumstellar matter – radio: abundances, planetary nebulae.

1 INTRODUCTION

Our Universe has been evolving for 13.8 Gyr. Over these years many stars formed and ended their lives enriching the interstellar medium (ISM), and in consequence enriching the Universe (Planck Collaboration 2014). Very few elements have been around since the beginning, formed by the Big Bang nucleosynthesis (BBN). BBN is responsible for the formation of most of the helium isotope (^{4}He) in the Universe, along with small amounts of deuterium (D), the helium isotope (^{3}He), and a very small amount of the lithium isotope (^{7}Li) (Alpher et al. 1948).

The predicted abundance (by number) of ^{3}He (relative to H) formed by the BBN (just after a few minutes after the Big Bang) is 1.0×10^{-5} (Karakas & Lattanzio 2014). This abundance depends only on the parameter of the current density of baryonic matter. The present interstellar ^{3}He abundance, as per all the light elements, comes from a combination of BBN and stellar nucleosynthesis (Wilson & Rood 1994). H II regions are young objects compared with the age of the Universe, and represent zero-age objects. Their ^{3}He abundance is the result of 13.8 Gyr of Galactic chemical evolution. In between is the Solar System, which traces abundances at the time of its formation, 4.6 Gyr ago.

Observed values in pre-solar material (Geiss 1993) and the ISM (Gloeckler & Geiss 1996) imply that ^{3}He/H=$(2.4\pm0.7)\times10^{-5}$. These values from the ISM and pre-solar material are approximately twice of the BBN, implying that the ^{3}He abundance has increased a little in the last 13.8 Gyr. On the other hand any hydrogen-burning zone of a star which is not too hot ($>7\times10^6$ K) will produce ^{3}He via the *p-p* chain, implying that stars with masses $<2.5\,M_\odot$ are net producers of ^{3}He. For these stars, *p-p* burning is rapid enough to produce D *in situ*, and enable the production of ^{3}He (D+ p $\rightarrow$ ^{3}He + γ). Stellar evolution models indeed predict the formation of ^{3}He in significant amounts by stars of 1–2.5 $M_\odot$, with an abundance of ^{3}He/H $> 10^{-4}$ (Bania et al. 2010), which would have raised the current ^{3}He abundance to ^{3}He/H$\sim 5\times10^{-5}$, substantially higher than observed (Karakas & Lattanzio 2014).

Galli et al. (1995) presented "The ^{3}He Problem". According to standard models of stellar nucleosynthesis there should be a ^{3}He/H abundance gradient in the Galactic Disk and the proto-solar ^{3}He/H value should be less than what is found in the present ISM. Observations of the ^{3}He abundance in H II regions show almost no enrichment above the BBN value (Rood et al. 1979; Bania et al. 2007).

⋆ E-mail: guzmanl@eso.org

For the ^{3}He problem to be solved, the vast majority of low-mass stars should fail to enrich the ISM. One suggestion to solve this problem is by adding extra mixing in the red giant branch (RGB) stage. This extra mixing adds to the standard first dredge-up to modify the surface abundances. Eggleton et al. (2006) estimate that while 90% of the ^{3}He is destroyed in 1 $M_\odot$ stars, only 40-60% is destroyed in a 2 $M_\odot$ star model, depending on the speed of mixing.

The abundance of ^{3}He can only be derived from the hyperfine transition at the rest frequency of 8.665 GHz. Detecting ^{3}He$^+$ in PNe challenges the sensitivity limits of all existing radio telescopes. Bania et al. (2010) observed a sample of 12 PNe, ^{3}He was detected in only 2 of them. NGC 3242 was observed with Effelsberg a 100m dish from the Max Planck Institute for Radio Astronomy (MPIfR) and the National Radio Astronomy Observatory (NRAO) 140-foot telescope, however the observations are inconsistent with each other. For the case of J320, ^{3}He was detected at a 4σ level with the NRAO Very Large Array (*VLA*). Composite ^{3}He$^+$ average spectrum for 6 PNe (NGC 3242, NGC 6543, NGC 6720, NGC 7009, NGC 7662, and IC 289), using Effelsberg, Arecibo and *GBT* observations, consistently show ^{3}He$^+$ emission at the $\sim$1 mK level. Guzman-Ramirez et al. (2013) observed 3 PNe (IC 418, NGC 6572, and NGC 7009) using the *VLA*, but no detections were made, and only upper limits were estimated.

In this letter we report a 5.7σ detection of the ^{3}He$^+$ line in the PN IC 418, using the National Aeronautics and Space Administration (NASA) DSS-63 antenna of Robledo de Chavela, Spain. In Sect. 2 the observations are described, while the results are presented in Sect. 3. The letter ends with a discussion about the derived abundance of ^{3}He$^+$, as well as the implications to the ^{3}He problem.

2 OBSERVATIONS

We used the DSS-63 antenna at the Madrid Deep Space Communications Complex (MDSCC), in Robledo de Chavela, Spain. MDSCC is part of the NASA's Deep Space Network; the observations were performed under the "Host Country Radio Astronomy" program. The antenna has a diameter of 70 m, which results in an angular resolution (half power beam width) of 115″, and a sensitivity of 1.25 Jy/K at 8.6 GHz.

We observed the position (RA, Dec)$_{J2000}$ = (05:27:28.2, -12:41:50), corresponding to the center of IC 418. The observations were carried out in different sessions between December 11, 2014 and March 24, 2015. The observing mode was position switching, which was done every 2 minutes, with the reference position at 12′ from the source in azimuth. Total on-source integration time was 1090 minutes (i.e., more than 18 hours). Data were corrected for atmospheric attenuation (all opacities measured were between 0.02 and 0.04) and elevation-dependent gain, based on a previously measured gain curve (Garcia-Miro et al. 2009).

We suffered a number of radio frequency interferences (RFIs) at fixed frequencies (8.330, 8.560, and 8.600 GHz). Fortunately we did not suffered from RFIs close to the ^{3}He$^+$ line. Furthermore, the bandpass is not totally uniform, which results in significantly higher system temperatures ($T_{\rm sys}$) at higher frequencies. While at the frequency of the H92α line (8.309 GHz) $T_{\rm sys}$ is only 22 K, at the frequency of the ^{3}He$^+$ line it is 210 K, which results in *rms* noise (1-sigma) increasing from 0.3 to 2.3 mK.

We used the new wideband backend (Rizzo et al. 2012), which provides a frequency resolution of 183 kHz ($\approx$ 6 km s^{-1} at 8.5 GHz) and an instantaneous bandwidth of 1.5 GHz; we therefore benefit from the totally usable bandwidth provided by the receiver, which goes approximately from 8.2 to 9.0 GHz.

Data was processed using CLASS, a part of the GILDAS software[1]. We subtracted the baselines around the detected radio recombination lines (RRLs) and around the ^{3}He$^+$ line to obtain an averaged spectra of every observing day. After that, spectra from all days have been combined in a single, final spectrum.

3 RESULTS

The Spirograph Nebula (IC 418, G215.2-24.2) has an elliptical ring shape, with a major axis of 14″ and a minor axis of 11″ (Ramos-Larios et al. 2012). It is surrounded by a low-level ionized halo, which is enshrouded in a neutral envelope with an angular size of about 2′ (Taylor & Pottasch 1987; Taylor et al. 1989). The ionized mass of the nebula is estimated at 0.06 $M_\odot$, and the mass of the progenitor at 1.7±0.3 $M_\odot$ (Morisset & Georgiev 2009).

The result of the observations are presented in two figures. In Fig. 1, the first detection of the ^{3}He$^+$ line in IC418 is presented. In this figure, a fraction of the spectra (approximately 40 MHz width) is depicted. The ^{3}He$^+$ line is clearly detected, together with the close RRLs, H114β and He114β. Although the intensity of the He114β line is quite large compared to the corresponding H line, the three lines are centred at the same radial velocity, which reinforces the reliability of the detections.

A number of other RRLs have also been observed, as indicated in the Fig. 2. All the lines: H92α, H91α, H116β, H115β, H114β, H132γ, H145δ, and their He counterparts are centred at 29 km s^{-1} and display similar line-widths. A Gaussian fitting to the detected RRLs are presented in Table 1.

Using the RRLs we analysed the local thermal equilibrium (LTE) and non-local thermal equilibrium (NLTE) conditions for IC 418 following Brocklehurst & Salem (1977) and Gordon & Sorochenko (2009). We found that LTE and NLTE conditions behave very similarly, NLTE conditions deviate less than 2.5% from LTE for the H132γ and H145δ lines. When comparing these LTE and NLTE values with the IC 418 observed ones, we found a small deviation of around 3mK, also seen in the H132γ and H145δ lines. We interpreted this deviation as an instrumental error. For a conservative approach we adopted this error in the measurement of the ^{3}He$^+$ line. For a safe LTE analysis, it is optimal to measure the continuum emission at the observed frequency with the same instrument used for the RRLs. Unfortunately, we were not able to do so, and have to infer the continuum. From Guzmán et al. (2009), the radio continuum flux density at 8.66 GHz is 400 mJy, scaling as $\nu^{-0.1}$ from $S_{\rm 5GHz} = 425 \pm 5$ mJy.

The ^{3}He$^+$ column density can be obtained using:

$$N(^3\mathrm{He}^+) = \frac{g_l + g_u}{g_u} \frac{8\pi k \nu^2}{hc^3 \mathrm{A}_{ul}} \int T_B(v) dv, \quad (1)$$

where g_u =1 is the g value or magnetic moment of the upper state, g_l =3 is the g value or magnetic moment of the lower state, A_{ul} =1.95436×10^{-12}s^{-1} (Gould 1994), and $T_B(v)$ is the brightness temperature profile of the line.

In order to measure the intensity of the ^{3}He$^+$ line, we used the task called tdv (from the CLASS software) which integrates the intensity of the line over the velocity range.

The flat or double-peaked line profile of the ^{3}He$^+$ line differs

[1] GILDAS is a radio astronomy software developed by IRAM. See `http://www.iram.fr/IRAMFR/GILDAS/`.

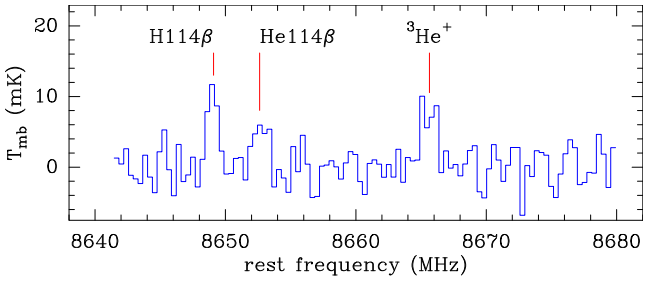

Figure 1. DSS-63 observations of the PN IC 418, showing part of the observed spectrum in a frequency range close to the $^3He^+$ line. This line and two close RRLs (H114β and He114β) are indicated. Abscissa is the rest frequency for a LSR velocity of 29 km s^{-1}. Data have been smoothed to a a resolution of 12.7 km s^{-1} (2 channels).

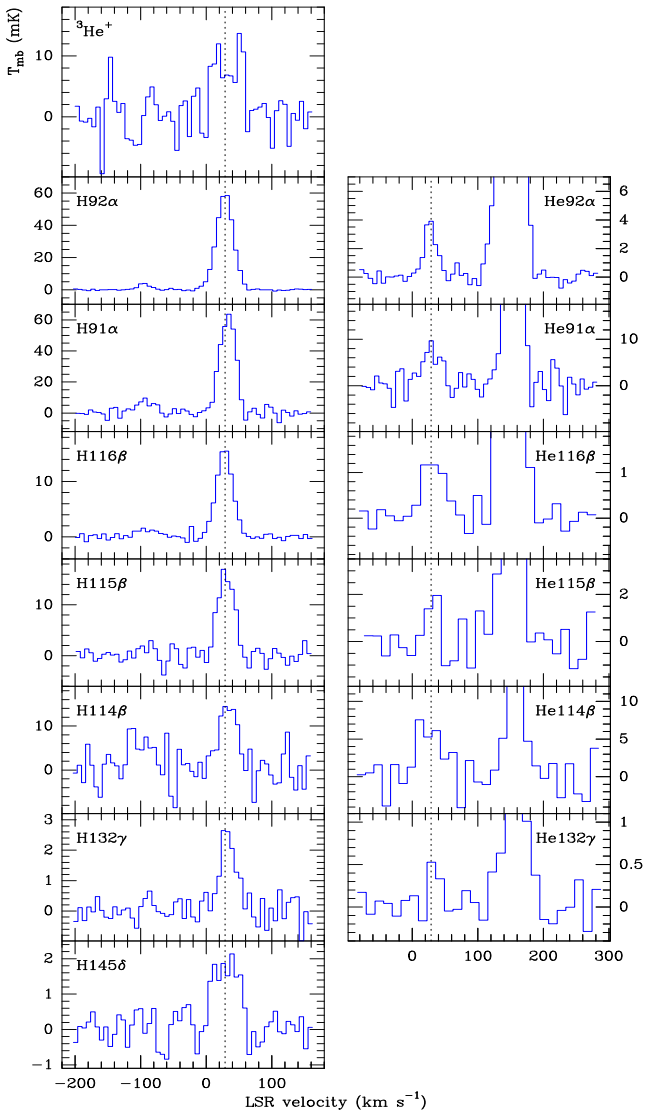

Figure 2. DSS-63 observations of the $^3He^+$ line and the RRLs detected in IC 418. Lines are indicated at the top left corner of each panel, $^3He^+$ and the H RRLs on the left, and the He RRLs on the right. The full resolution is used, with a channel width of 6.3 km s^{-1} at 8.66 GHz except for H132γ and the He RRLs that have been smoothed to a resolution of 12.7 km s^{-1} (2 channels) to improve the visibility. To ease the comparison, a dashed line at 29 km s^{-1} is over-plotted.

Table 1. $^3He^+$ line and radio recombination lines detected in the PN IC 418.

Line	T_{mb} (mK)	Area (mK km s^{-1})	Δv (km s^{-1})
$^3He^+$	10.6±3.0	369.8±64.7	–
H92α	59.8±0.6	1925.8±15.0	30.2±0.2
He92α	3.6±0.5	72.0±8.4	21.9±1.9
H91α	64.3±3.0	1884.1±59.4	27.5±0.9
He91α	7.1±3.3	210.7±53.5	28.3±6.6
H116β	16.0±1.3	507.3±26.5	29.6±1.9
He116β	1.3±0.5	59.2±29.4	40.7±23.4
H115β	16.7±1.6	507.1±32.3	28.4±1.9
He115β	2.1±1.4	48±23	32.3±7.1
H114β	14.5±3.7	470.5±77.3	30.4±5.5
He114β	5.5±4.0	121.5±85.2	36.0±12.8
H132γ	2.6±0.5	78.9±10.8	28.3±4.8
He132γ	0.6±0.3	9.1±4.8	12.5±7.7
H145δ	2.0±0.5	87.9±11.8	41.3±5.3

from the gaussian profiles of the H and He recombination lines. The full width at zero maximum of the lines agree, but the outer peaks of the $^3He^+$ line are lacking from the recombination lines. We therefore separated the inner and outer parts of the line profiles through a triple gaussian fit. The inner component, with a FWHM of 18 km s^{-1}, consistent with the recombination lines, is used as a lower value to the line intensity. The full integrated intensity is used as the upper value. We then used the beam filling factor (bff) to derive the observed beam-averaged brightness temperature T_{mb} (Garcia-Miro et al. 2009).

The number density of $^3He^+$ atoms, $n(^3He^+)$, can be obtained by dividing the column density $N(^3He^+)$ by the averaged optical path, $< \Delta s >$, through the source. Representing a PN as a homogeneous sphere of radius $R = \theta_s D$, where D is the distance, the optical path at angle from the centre θ is $\Delta s(\theta) = 2\sqrt{R^2 - (\theta D)^2}$, and the optical path averaged over the source becomes $< \Delta s >= \pi R/2 = \pi\theta_s D/2$.

The expression for $n(^3He^+)$ is then

$$\frac{n(^3\mathrm{He}^+)}{\mathrm{cm}^{-3}} = 44.6\left(\frac{T_{mb}\,\Delta v}{\mathrm{mK\,km\,s^{-1}}}\right)\left(\frac{D}{\mathrm{kpc}}\right)^{-1}\left(\frac{\theta_s}{''}\right)^{-3}\left(\frac{\theta_b}{57.5''}\right)^{2}\left(1+\frac{\theta_s^2}{\theta_b^2}\right) \quad (2)$$

Table 1 presents the line peak (T_{mb}), the integrated intensity, and the width (Δv) of all the lines observed. For the $^3He^+$ we integrated the intensity of the line; for the RRLs we fitted a gaussian to estimate their intensities. The intensity ratios of the Hnα and Hnβ are consistent with model predictions to within 10%, for an emission measure of EM$\sim 7\times10^6$ pc cm^{-6} (Hjellming et al. 1969). The line-to-continuum ratio ~4.5%, is also consistent with this EM. This gives confidence in the bandpass and flux calibration.

To calculate the fractional ^{3}He abundance we divide by the H^+ density. The H^+ density was modelled using Cloudy_3D (Morisset 2006). In this Cloudy_3D model for IC418 the nebula is an ellipsoid with a small eccentricity. Because of the small eccentricity, a spherical version of the nebula was also tested, giving similar results, with the caveat that the radial density profile is not uniform, two shells were needed. From that model, a mean H+ density can be derived. The value presented in Table 2 was taken from Morisset & Georgiev (2009). The distance used was 1.3kpc (Guzmán et al. 2009).

From the detailed model of IC 418 described by Morisset & Georgiev (2009), the Ionisation Correction Factor (ICF) of He^+ is 1.45 (taking into account the presence of an He^0 region). This

Table 2. The ^{3}He abundance in the PN IC 418. The upper row uses the central component of the ^{3}He line only; the bottom row uses the full integrated line profile. These are used as lower and upper values respectively. An ICF (He^+) of 1.45 was used.

D (kpc)	θ_s ($''$)	$T_{mb}\Delta v$ (mK km s^{-1})	$n(H^+)$ (cm^{-3})	$n(^3He^+)$ (cm^{-3})	^{3}He/H (10^{-3})
1.3±0.4	7	109.1±42.3	9.3×10^3	11.1±4.9	1.74±0.8
1.3±0.4	7	369.8±64.7	9.3×10^3	37.5±10.5	5.8±1.7

yields an abundance of ^{3}He/H=$1.74\pm0.8\times10^{-3}$ for the lower limit, and $5.8\pm1.7\times10^{-3}$ for the upper limit.

The recombination lines allow us to estimate the total He/H ratio (Roelfsema et al. 1987). We calculated the ratio of the line strength integrated over the profile, for the five available line couples (He91α/H91α, etc). The ratios are multiplied by the ICF for helium of 1.45, and divided by 1.07 to account for the slightly different radiative recombination rates of hydrogen and helium. He92α is a factor of three fainter than expected and we suspect a fitting error, while He114β is too faint for a reliable value. The remainder give He/H= 0.15 ± 0.03. ^{3}He accounts for 4% of the helium in IC 418.

4 DISCUSSION

4.1 Origin of the $^3He^+$ emission

Three aspects of the current data needs to be considered. First, the derived $^3He^+$ abundance is well above model expectations. Second, the upper value for the $^3He^+$ abundance is only a little lower than the earlier 3-σ VLA upper limit. Third, although the full width of the $^3He^+$ line is consistent with the optical expansion velocity of IC 418, the profile differs from that of the recombination lines, peaking at the outermost velocities.

A double-peaked profile could arise from an expanding detached shell, which is larger than the beam. In this case, the outer components of the profile, which differ from the recombination lines, come from this large region, whilst the central part of the profile arises from the inner, ionized nebula. Balser et al. (1999) also proposed a contribution from a large, low density halo. The emission in the $^3He^+$ hyperfine line scales with $\int n\,dr$ (column density), and that of recombination line with $\int n^2\,dr$. Therefore, a low density but high mass halo could explain the difference in profiles.

Two other PNe have reported $^3He^+$ detections: J320 Balser et al. (2006) and NGC 3242 Balser et al. (1997, 1999, 2006). Both have double peaked profiles, similar to IC 418 (Fig. 3). Both objects have haloes, in the case of NGC 3242 possibly as large as 18 by 24 arcmin diameter Bond (1981). Whether helium in such a halo could be photo-ionized by the star is not clear. NGC 3242 has an inner shell and an outer elliptical envelope, but the inner shell is optically thick to He^+ ionizing photons (Ruiz et al. 2011).

If part of the line arises from a halo, then the fractional abundance should be calculated excluding this part. The reason for this is that the ionized mass derived from recombination or free-free emission, as used in the calculations, is not sensitive to such haloes. The total mass of ionized haloes is very poorly constrained. We therefore consider the low value for the ^{3}He/H ratio for IC 418, which was derived for the line component coinciding with the recombination lines, as more likely.

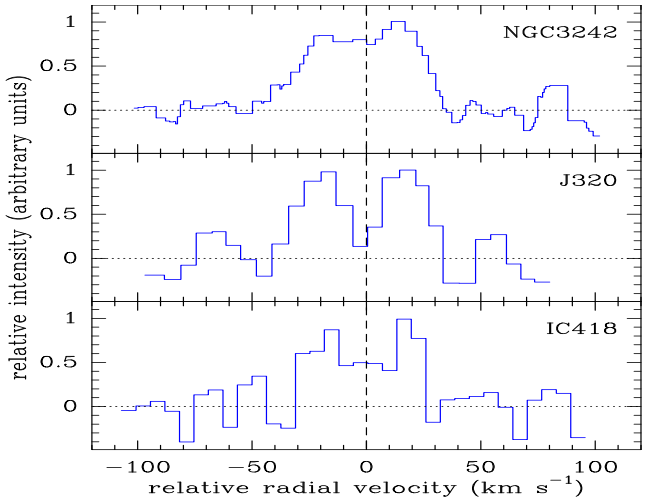

Figure 3. All the $^3He^+$ line detected in planetary nebulae. The sources are NGC 3242 (Balser et al. 1999), J320 (Balser et al. 2006), and IC 418 (this work). In order to facilitate the comparison, the abscissa is presented as radial velocities relative the LSR systemic velocity of each source (dashed-line), and the intensity scale as fractions of the peak intensity of each source.

4.2 Zeeman splitting

Zeeman splitting in the $^3He^+$ line is similar to that of the HI line. The line frequency moves by 1.399 kHzmG^{-1}, or 0.48 km s^{-1} mG^{-1}. The two σ components are separated by twice this. For a typical field strength within PNe of a few mG Sabin et al. (2007), the line shifts in frequency by one to a few km s^{-1}. This is insufficient to explain the difference in line profile.

4.3 Hyperfine maser

Deguchi & Watson (1985) show that the spin temperature of $^3He^+$ can go negative only if $[He^{++}/He^+]>> 0$. The inversion in this case is driven by ^{4}He Lyα absorption. This effect requires very high excitation. Some PNe do contain regions of such high ionization.

The outer peaks of the $^3He^+$ profiles could show the effect of amplification. The inner peak would give the actual abundance, unaffected by non-thermal amplification. The preferred value for the $^3He^+$ fractional abundance is again the lower value derived above.

4.4 Stellar evolution

The contribution of PNe to the ^{3}He abundance is crucial for understanding the Galactic chemical evolution. Figure 4 shows the ^{3}He abundances of the PN IC 418 (both purple crosses). For comparison the upper limits calculated from Guzman-Ramirez et al. (2013) observations are presented using the red arrows. Balser et al. (1997) observations are shown in green: the cross represents J320 and the arrows are the upper limits, where the mass estimates are from Galli et al. (1997). The stellar evolution models are also presented in Figure 4.

Even for the lower value for IC 418, which we consider as more likely, the abundance is above the model calculations for any mass. This present problems for models which invoke deep mixing (purple dashed-line) Boothroyd & Sackmann (1999). The STARS models (blue line) with extra mixing via thermohaline convection by Charbonnel & Zahn (2007) come closest.

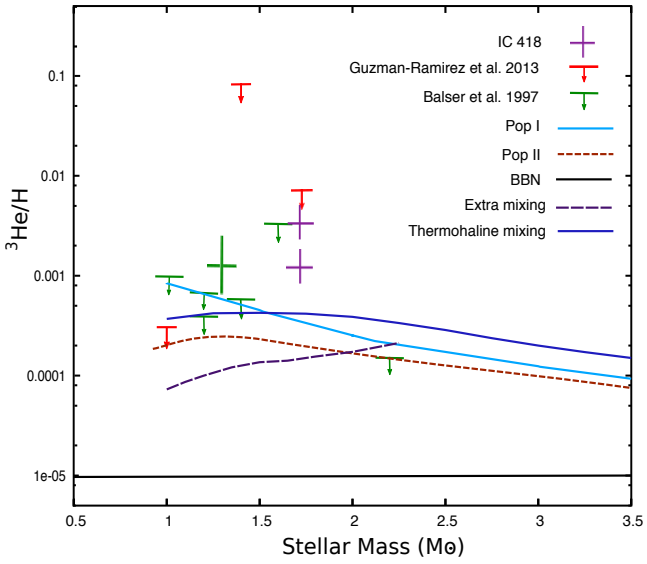

Figure 4. Abundances of ^{3}He (relative to H) for the PN IC 418 (both purple crosses, for upper and lower estimate), the size of the bars correspond to the uncertainties. Red arrows are the upper limits from Guzman-Ramirez et al. (2013). The green cross represents J320 and the green arrows represent the sample of 6 PNe from Balser et al. (1997). The curves for Pop I (light-blue line) and II (red dashed-line) show the standard abundance of ^{3}He taken from Weiss et al. (1996). The purple dashed-line labelled Extra mixing represents the results of models including deep mixing by Boothroyd & Sackmann (1999), and the blue line shows the stellar models using thermohaline mixing (Charbonnel & Zahn 2007). The black line is the primordial value of ^{3}He/H from the BBN (Karakas & Lattanzio 2014).

5 CONCLUSIONS

We have detected the $^3He^+$ line towards the PN IC 418 using the DSS-63 antenna. We derive $n(^3He^+)$=11±5–38±11cm^{-3}, corresponding to ^{3}He/H=1.7±0.8–5.8±1.7×10^{-3}. We have some preference for the lower range, which is derived using the central component of the line only. The outer component may arise in a extended low density halo.

The values exceed prediction from stellar evolution models, especially those invoking deep mixing. The lower limit is a factor of 2 above the thermohaline model and we may be approaching consistency with it. However, the large amounts of ^{3}He produced in these models is at odds with the abundance of ^{3}He observed in the ISM and the Solar System (∼10^{-5}). The ^{3}He problem lingers.

ACKNOWLEDGMENTS

This work is based on observations made with the DSS-63 antenna at the MDSCC, under the "Host Country Radio Astronomy" program. LGR thanks Arturo Manchado for bringing the DSS-63 antenna to her attention. LGR is co-funded under the Marie Curie Actions of the European Commission (FP7-COFUND). CM acknowledges the UNAM project PAPIIT-107215

REFERENCES

Alpher R. A., Bethe H., Gamow G., 1948, Physical Review, 73, 803
Balser D. S., Bania T. M., Rood R. T., Wilson T. L., 1997, ApJ, 483, 320
Balser D. S., Goss W. M., Bania T. M., Rood R. T., 2006, ApJ, 640, 360
Balser D. S., Rood R. T., Bania T. M., 1999, ApJL, 522, L73
Bania T. M., Balser D. S., Rood R. T., Wilson T. L., LaRocque J. M., 2007, ApJ, 664, 915
Bania T. M., Rood R. T., Balser D. S., 2010, in Charbonnel C., Tosi M., Primas F., Chiappini C., eds, IAU Symposium Vol. 268 of IAU Symposium, Measurements of ^{3}He in Galactic HII regions and planetary nebulae. pp 81–90
Bond H. E., 1981, Public. of the Astron. Soc. Pac., 93, 429
Boothroyd A. I., Sackmann I.-J., 1999, ApJ, 510, 232
Brocklehurst M., Salem M., 1977, Computer Physics Communications, 13, 39
Charbonnel C., Zahn J.-P., 2007, A&A, 467, L15
Deguchi S., Watson W. D., 1985, ApJ, 290, 578
Eggleton P. P., Dearborn D. S. P., Lattanzio J. C., 2006, Science, 314, 1580
Galli D., Palla F., Ferrini F., Penco U., 1995, ApJ, 443, 536
Galli D., Stanghellini L., Tosi M., Palla F., 1997, ApJ, 477, 218
Garcia-Miro C., Moll E., Vazquez M., Kuiper T. B. H., 2009, Astronomische Nachrichten, 330, 137
Geiss J., 1993, in Prantzos N., Vangioni-Flam E., Casse M., eds, Origin and Evolution of the Elements Primordial abundances of hydrogen and helium isotopes.. pp 89–106
Gloeckler G., Geiss J., 1996, Nature, 381, 210
Gordon M. A., Sorochenko R. L., eds, 2009, Radio Recombination Lines Vol. 282 of Astrophysics and Space Science Library
Gould R. J., 1994, ApJ, 423, 522
Guzmán L., Loinard L., Gómez Y., Morisset C., 2009, AJ, 138, 46
Guzman-Ramirez L., Pineda J. E., Zijlstra A. A., Stancliffe R., Karakas A., 2013, MNRAS, 432, 793
Hjellming R. M., Andrews M. H., Sejnowski T. J., 1969, Astrophys. Lett., 3, 111
Karakas A. I., Lattanzio J. C., 2014, Publications of the Astronomical Society of Australia, 31, 30
Morisset C., 2006, in Barlow M. J., Méndez R. H., eds, Planetary Nebulae in our Galaxy and Beyond Vol. 234 of IAU Symposium, Cloudy_3D, a new pseudo-3D photoionization code. pp 467–468
Morisset C., Georgiev L., 2009, A&A, 507, 1517
Planck Collaboration e. a., 2014, A&A, 571, A1
Ramos-Larios G., Vázquez R., Guerrero M. A., Olguín L., Marquez-Lugo R. A., Bravo-Alfaro H., 2012, MNRAS, 423, 3753
Rizzo J. R., Pedreira A., Gutiérrez Bustos M., et al. 2012, A&A, 542, A63
Roelfsema P. R., Goss W. M., Whiteoak J. B., Gardner F. F., Pankonin V., 1987, A&A, 175, 219
Rood R. T., Wilson T. L., Steigman G., 1979, ApJL, 227, L97
Ruiz N., Guerrero M. A., Chu Y.-H., Gruendl R. A., 2011, AJ, 142, 91
Sabin L., Zijlstra A. A., Greaves J. S., 2007, MNRAS, 376, 378
Taylor A. R., Gussie G. T., Goss W. M., 1989, ApJ, 340, 932
Taylor A. R., Pottasch S. R., 1987, A&A, 176, L5
Weiss A., Wagenhuber J., Denissenkov P. A., 1996, A&A, 313, 581
Wilson T. L., Rood R., 1994, Annual Review of Astron and Astrophys, 32, 191

This paper has been typeset from a TEX/ LATEX file prepared by the author.